Shock Waves in Dynamic Cavity Expansion

Tal Cohen[1]
e-mail: btal@tx.technion.ac.il

Rami Masri

David Durban

Faculty of Aerospace Engineering,
Technion,
Haifa 32000, Israel

High velocity cavitation fields are investigated in the context of large strain J_2 plasticity with strain hardening and elastic compressibility. The problem setting is that of an internally pressurized spherical cavity, embedded in an unbounded medium, which grows spontaneously with constant velocity and pressure. Expansion velocity is expected to be sufficiently high to induce a plastic shock wave, hardly considered in earlier dynamic cavitation studies. Jump conditions across singular spherical surfaces (shock waves) are fully accounted for and numerical illustrations are provided over a wide range of power hardening materials. Simple formulae are derived for shock wave characteristics and for the asymptotic behavior within near cavity wall boundary layer.
[DOI: 10.1115/1.4000914]

Keywords: dynamic cavity expansion, spherical cavitation, plastic shock waves

1 Introduction

A considerable amount of work has been devoted to dynamic cavitation fields induced in elastoplastic media by an internally pressurized spherical cavity (a detailed review of earlier studies was given recently by Masri and Durban [1]). However, cavity expansion velocities have been limited to a moderate range of about $m<0.4$, m being the ratio of expansion velocity to wave speed in long elastic rods. At higher radial expansion velocities, emergence of a new plastic shock wave becomes possible and solution of field equations is more complicated by the associated jump conditions across that shock wave.

In this paper, we investigate steady-state self-similar dynamic cavitation fields in spherical geometry with velocities of up to $m=0.7$. Constitutive response is described by the finite strain J_2 theory of plasticity, which includes elastic compressibility and strain hardening. The governing system of equations is briefly recapitulated from Masri and Durban [1]. Subsequent analysis centers on two ordinary nonlinear differential equations for radial distribution of stress components.

The location of singular surfaces is determined by a new relation (2.10), which generalizes the known small-strain plastic wave speed [2]. Hugoniot jump conditions are discussed in Sec. 3 in conjunction with radial displacement continuity and singularity conditions on each side of shock wave. The rigid/elastic interface conditions and small-strain elastic field (up to onset of initial yield) are presented in Sec. 4.

Next, in Sec. 5, we investigate in detail the plastic shock wave characteristics. Closed form approximations are derived for the representative effective stress within the shock wave, for stresses discontinuity ratio across the shock, and for shock wave location in terms of uniaxial stress-strain relation. Dependence of shock intermediate Mises stress on hardening index is shown to be predicted very well by formula (5.8).

The numerical results are presented in Sec. 6 for radial profiles of field variables (stresses, velocity, and density) and for dependence of cavitation pressure on cavity expansion velocity. Illustrative data are provided over a wide range of material parameters (yield stress, hardening index, and Poisson ratio). The emergence of plastic shock is clearly observed, with increasing level of discontinuities, as m increases. Location of both rigid/elastic interface and plastic shock wave approach cavity wall with higher values of m. Dependence of cavitation pressure on expansion velocity shows little sensitivity to hardening index but decreases with elastic compressibility.

The paper concludes (Sec. 7) with an asymptotic analysis of the near wall boundary layer. Simple formulae are obtained for radial profiles of stresses and shown to be in good agreement with accurate numerical calculations.

The analysis and results given here are applicable to studies of plastic shock waves behavior and to penetration depth estimation of high velocity projectiles. Existing studies of dynamic spherical cavitation in plastic solids (Hunter and Crozier [3]) are here generalized by considering the complete J_2 large strain theory with strain hardening and high expansion velocities.

2 Governing Equations

Consider the expansion of a spherical cavity, of current radius A due to uniform internal pressure p under steady-state self-similar conditions (Fig. 1). The surrounding material is an unbounded Mises plastic solid with the spherically symmetric active Cauchy components $\sigma_r, \sigma_\theta = \sigma_\phi$, defined in a (R, θ, ϕ) spatial spherical system of coordinates. The normalized radial coordinate is $\xi = R/A$ and the normalized radial velocity is $V = \dot{R}/\dot{A}$, where the superposed dot denotes differentiation with respect to time. For steady-state expansion it is required that the cavity expansion velocity $\dot{A}$ is constant and that all field variables depend only on ξ.

Masri and Durban [1] showed (Eqs. (17) and (19) therein) that for a hypoelastic J_2 compressible Mises solid with arbitrary strain hardening, the field equations admit two closed form relations for the density ratio ρ/ρ_o and the material velocity V, namely,

$$\frac{\rho}{\rho_o} = e^{-\Theta}, \quad \Theta = 3\beta\Sigma_h, \quad \beta = 1 - 2\nu \tag{2.1}$$

$$V = \xi(1 - e^{-\Phi}), \quad \Phi = \frac{3}{2}\varepsilon - \frac{1}{2}\beta\Sigma \tag{2.2}$$

Hence, ρ is the current density, ρ_o is the undeformed reference density, ν is the Poisson ratio, Σ_h is the hydrostatic stress normalized by the elastic modulus, and ε denotes the total strain, which is a known function of the Mises stress Σ (again normalized by E). Thus $(\Sigma_r, \Sigma_\theta, \Sigma) = (\sigma_r, \sigma_\theta, \sigma_e)/E$, where $\sigma_e = \sigma_\theta - \sigma_r$, $\Sigma_h = (\Sigma_r + 2\Sigma_\theta)/3$, and $\varepsilon = \Sigma + \varepsilon_P$, where ε_P denotes the effective plastic strain.

[1]Corresponding author. This work is based on a part of a M.Sc thesis to be submitted to the Technion.

Contributed by the Applied Mechanics Division of ASME for publication in the JOURNAL OF APPLIED MECHANICS. Manuscript received April 12, 2009; final manuscript received October 22, 2009; published online April 9, 2010. Assoc. Editor: Vikram Deshpande.

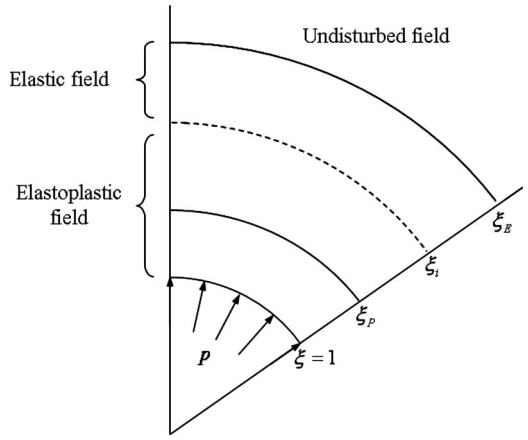

Fig. 1 Diagram of the field induced by self-similar expansion of a spherical cavity (with current radius *A*) in an unbounded Mises medium in the presence of an elastoplastic shock wave. *p* is the applied pressure and $\xi=R/A$ is the nondimensional radial coordinate. ξ_E and ξ_P represent the rigid/elastic and the plastic wave fronts, respectively, while ξ_i denotes the elastoplastic interface where $\sigma_e=\sigma_y$.

The two remaining differential equations that govern the spherical expansion process are (Eqs. (20) and (21) in Masri and Durban [1])

$$\beta\Sigma_r' + \frac{\beta}{2}\Sigma' + \frac{1}{2}\varepsilon' = \frac{1}{\xi}(1 - e^{\Phi}) \tag{2.3}$$

$$\Sigma_r' - m^2\xi^2(\beta\Sigma_r' + \beta\Sigma' - \varepsilon')e^{-\Theta-2\Phi} = \frac{2}{\xi}\Sigma \tag{2.4}$$

with the nondimensional cavity expansion velocity defined by

$$m = \frac{\dot{A}}{\sqrt{E/\rho_o}} \tag{2.5}$$

and the superposed prime denoting differentiation with respect to ξ.

As they stand, Eqs. (2.3) and (2.4) need to be solved for Σ_r and Σ as functions of ξ. Notice that Φ depends only on Σ while

$$\Theta + 2\Phi = 3\beta\Sigma_r + 3\varepsilon + \beta\Sigma \tag{2.6}$$

The purpose of the present work is to examine solutions of Eqs. (2.3) and (2.4) for cavitation fields at high expansion velocities, which induce a plastic wave front.

While in this formulation the dependence of ε_p on σ_e has been left arbitrary, a broad range of plastic response is covered by the power law

$$\varepsilon_p = 0 \quad \text{for} \quad \sigma_e < \sigma_y$$
$$\varepsilon_p = \frac{\sigma_y}{E}\left(\frac{\sigma_e}{\sigma_y}\right)^{1/n} - \frac{\sigma_e}{E} \quad \text{for} \quad \sigma_e \geq \sigma_y \tag{2.7}$$

where σ_y is the yield stress and n is the hardening index. Relation (2.7) is employed here for numerical illustrations of dynamic spherical cavitation fields.

To sum up, we have two differential equations (2.3) and (2.4) with two unknowns (Σ_r,Σ) whose radial variation with the independent variable ξ should be determined. The profiles of density (ρ) and velocity (V) are then obtained from relations (2.1) and (2.2), respectively.

While governing equations are identically satisfied within the undisturbed zone $(\xi_E<\xi<\infty)$, integration of the system starts at the rigid/elastic interface where

$$\xi = \xi_E: \quad \Sigma = 0, \quad \Sigma_r = 0, \quad (\rho = \rho_o, \ V = 0) \tag{2.8}$$

up to the cavity wall where

$$\xi = 1: \quad \Sigma_r = -P, \quad \Sigma \to \infty, \quad (\rho \to 0, \ V = 1) \tag{2.9}$$

Here, $P=p/E$ is the applied cavitation pressure normalized with respect to the elastic modulus. The problem lies in finding the value of P for which a solution exists.

Before performing numerical integration it is necessary to determine the conditions of possible singularities of Eqs. (2.3) and (2.4). To this end, we use the identity $\Sigma'=h\varepsilon'$ where $h=d\Sigma/d\varepsilon$ is the nondimensional tangent modulus of the stress-strain curve determined by the tension test. The determinant of the coefficients of first-order derivatives (Σ_r',Σ') on left hand side of Eqs. (2.3) and (2.4) vanishes when

$$\beta m^2\xi^2 = \frac{1+\beta h}{3-\beta h}e^{\Theta+2\Phi} \tag{2.10}$$

which dictates the radial location ξ of singular spherical surfaces.

Shock waves are identified as singular surfaces (Eq. (2.10)), which permit discontinuities of field variables, governed by the Hugoniot jump conditions together with continuity of the circumferential strain. Since Eqs. (2.3) and (2.4) are nonhomogeneous, it can be shown by basic algebraic reasoning that the derivatives (Σ_r',Σ') will become unbounded at the shock location unless the equality

$$1 - e^{\Phi} = \beta\Sigma\frac{3-\beta h}{1+\beta h} \tag{2.11}$$

is satisfied. However, for conventional metals that equality is not applicable over range of interest.

Relation (2.10) reduces to small-strain plastic wave speed $(C_P = m\xi_P)$, in steady-state cavitation,

$$\beta C_P^2 = \frac{1+\beta h}{3-\beta h} \tag{2.12}$$

derived by Hopkins [2] (Eq. (6.43)) with an earlier reference to Luntz [4] and discussed in later studies within the context of small-strain plasticity [5]. In the absence of hardening $(h=0)$, we recover the standard bulk wave speed $3\beta C_P^2=1$.

As we shall see in next sections, there are two different types of discontinuities in the spherical cavitation fields. At the rigid/elastic interface $\xi=\xi_E$ all field variables pass continuously with Eqs. (2.3) and (2.4) being homogenous while the derivatives Σ_r' and Σ' remain finite but discontinuous. At the plastic shock discontinuity $(\xi=\xi_P)$, there is a possibility of finite jump in values of field variables, Eqs. (2.3) and (2.4) are nonhomogeneous and stress derivatives may become unbounded on both sides of the shock wave. No discontinuity of field variables has been encountered at the elastic/plastic interface $(\xi=\xi_i)$ unless the plastic wave coincides with elastic/plastic interface. In fact, for solids that do not exhibit a definite yield point (such as the Ramberg–Osgood relation) there is no elastic/plastic interface.

3 Jump Conditions

When singularity arises and discontinuity in system variables is possible the governing field equations must be replaced by finite (jump) relations. The variables, which admit discontinuities are (ρ,V,Σ_r,Σ) two of which (ρ,V) are given by Eqs. (2.1) and (2.2).

Two fundamental conditions are the Hugoniot jump conditions, requiring conservation of mass and momentum,

$$\left[\!\left[\frac{\rho}{\rho_o}(V_W - V)\right]\!\right] = 0$$

$$\left[\!\left[\Sigma_r + m^2\frac{\rho}{\rho_o}(V_W - V)V\right]\!\right] = 0$$

where V_W is the wave speed. When a wave emerges, at a constant material radius $\xi=\xi_W$, then $V_W=\xi_W$ and the Hugoniot relations can be rewritten as

$$\left[\!\left[\frac{\rho}{\rho_o}(\xi_W - V)\right]\!\right] = 0 \tag{3.1}$$

$$\left[\!\left[\Sigma_r + m^2\frac{\rho}{\rho_o}(\xi_W - V)V\right]\!\right] = 0 \tag{3.2}$$

A third restriction on permissible jumps is continuity of the radial displacement across the shock. However, continuity of the radial displacement translates to continuity of the circumferential strain, within framework of J_2 theory of plasticity [1]

$$\left[\!\left[-\nu\Sigma_r + (1-\nu)\Sigma_\theta + \frac{1}{2}\varepsilon_P\right]\!\right] = 0$$

which, in view of Eq. (2.6), can be written as

$$[\![\Theta + \Phi]\!] = 0 \tag{3.3}$$

with Θ and Φ defined in Eqs. (2.1) and (2.2).

To sum up, we have the three jump conditions (3.1)–(3.3) at each location of the singularity surface, $\xi=\xi_W$, along with the singularity condition (2.10), which is imposed on both sides of the wave (denoted as $\xi=\xi_W^-, \xi_W^+$). Thus we rewrite Eq. (2.10) as

$$\beta m^2 \xi_W^2 = \left.\frac{1+\beta h}{3-\beta h}e^{\Theta+2\Phi}\right|_{at\ \xi_W^-\ \text{and}\ \xi_W^+} \tag{3.4}$$

for the two distinct requirements. Subsequently values on the inner side of the jump (closer to the cavity wall) are denoted with a superscripted $(-)$ and the values on the outer side with a superscripted $(+)$.

Relations (3.1)–(3.4), together with boundary data in Eqs. (2.8) and (2.9), enable a complete numerical solution for variables $(\Sigma_r, \Sigma, \rho, V)$ in the presence of discontinuities. A helpful observation in this context is that relations (2.1) and (2.2) hold on both sides of the wave. In fact inserting relations (2.1) and (2.2) into condition (3.1) generates the displacement continuity (3.3), implying that the hydrostat (2.1) together with Eq. (2.2) are equivalent to requirement (3.3).

4 Elastic Field $\xi_i < \xi < \xi_E$

At the far field $(\xi > \xi_E)$ material is undisturbed with $V=0$, $\rho=\rho_o$, and all stress components vanish. Thus, the location of rigid/elastic interface is found from singularity condition (3.4) at $\xi=\xi_E^+$

$$m^2\xi_E^2 = \frac{1+\beta}{\beta(3-\beta)} = \frac{1-\nu}{(1-2\nu)(1+\nu)} \tag{4.1}$$

in agreement with the linear elasticity result for wave speed $C_E=m\xi_E$. It is a matter of ease to show that there are no jumps at the rigid/elastic interface so $\rho^-=\rho_o$ with vanishing stresses and velocity at ξ_E^-.

It follows that Eqs. (2.3) and (2.4) are homogeneous at $\xi=\xi_E^-$ implying finite values of derivatives of field variables. In fact, Durban and Masri [6] cast the small-strain elastic solution for $\xi_i < \xi \le \xi_E$ into the form

$$\Sigma_r = \frac{2C}{3\xi_E^3}\left(\left(\frac{\xi_E}{\xi}\right)^2 + \frac{\xi_E}{\xi} + \frac{3-\beta}{2\beta}\right)\left(1 - \frac{\xi_E}{\xi}\right) \tag{4.2}$$

$$\Sigma = \frac{C}{\xi_E^3}\left(\left(\frac{\xi_E}{\xi}\right)^3 - \frac{\xi_E}{\xi}\right) \tag{4.3}$$

Elastic field consistency implies that $\rho=\rho_o$ and material velocity is accordingly

$$V = (1+\nu)\xi\Sigma \tag{4.4}$$

This solution is valid up to the elastic/plastic interface $\xi=\xi_i$, where $\Sigma=\Sigma_y$ with $\Sigma_y=\sigma_y/E$ denoting the nondimensional yield stress. The constant C is determined by the numerical solution of the entire elastoplastic zone up to the cavity wall.

At the elastic/plastic interface, all field variables remain continuous, although jumps in first-order derivatives are encountered. Thus, integration of governing equations proceeds from ξ_i^- inwards with stress depending only on constant C.

5 Elastoplastic Field $1 < \xi < \xi_i$

When $\xi=\xi_i$ $(\sigma_e=\sigma_y)$, plasticity sets in and integration of the governing equations is performed numerically. The values of constant C are iterated until boundary data at the cavity wall is met (when $\Sigma\to\infty$). The corresponding cavitation pressure is then given by $P=-\Sigma_r(\xi=1)$. For cavity expansion velocities below a critical value, no plastic wave will develop and several examples of these fields are illustrated in Masri and Durban [1]. However, with cavity expansion velocities above the critical value, singularity of the equations arises and a new discontinuity, a plastic shock wave has to be considered. The location of this wave $(\xi=\xi_P)$ is determined by condition (2.10), namely,

$$\beta m^2 \xi_P^2 = \left.\frac{1+\beta h}{3-\beta h}e^{\Theta+2\Phi}\right|_{\xi=\xi_P^+,\xi_P^-} \tag{5.1}$$

where the right hand side of Eq. (5.1) is evaluated on both sides of the wave. Equations (2.3) and (2.4) are nonhomogeneous, at $\xi=\xi_P^-, \xi_P^+$ implying that the derivatives $(\Sigma_r', \Sigma', \rho', V')$ may become unbounded and that the variables $(\Sigma_r, \Sigma, \rho, V)$ admit possible discontinuities across the wave, indicating the existence of a plastic shock wave. Jump conditions (3.1)–(3.4) need now to be implemented in numerical procedure to facilitate solution in the presence of a plastic shock.

Instructive insight into plastic shock wave characteristics can be obtained by a fairly simple analysis, exposing behavior of central parameters at ξ_P. We start by rewriting Eq. (2.10) on each side of the shock as

$$\beta m^2 \xi_P^2 e^{-\Theta-\Phi} = \left.\frac{1+\beta h}{3-\beta h}e^{\Phi}\right|_{\xi=\xi_P^-,\xi_P^+} \tag{5.2}$$

but since $[\![\Theta+\Phi]\!]=0$, by Eq. (3.3), r.h.s. of Eq. (5.2) should be continuous as well

$$\left[\!\left[\frac{1+\beta h}{3-\beta h}e^{\Phi}\right]\!\right] = 0 \tag{5.3}$$

It follows that the function $f(\Sigma)$ defined by

$$f(\Sigma) = \frac{1+\beta h}{3-\beta h}e^{\Phi} \tag{5.4}$$

must exhibit an extremum within the range of interest $(\Sigma^+ \le \Sigma \le \Sigma^-)$, namely,

$$\frac{df}{d\Sigma} = 0 \to \Sigma = \Sigma_P \tag{5.5}$$

where Σ_P is an intermediate value of Σ, characterizing the shock $(\Sigma^+ \le \Sigma_P \le \Sigma^-)$. The existence of such an extremum of $f(\Sigma)$ de-

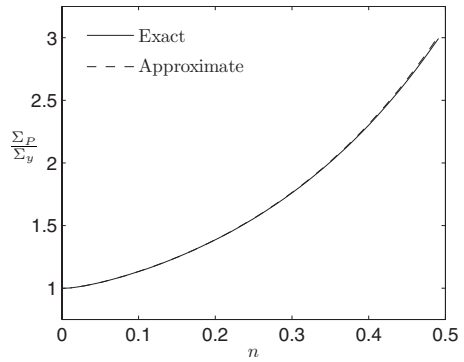

Fig. 2 Comparison of shock intermediate effective stress values from exact solution of Eq. (5.6) with approximate value from Eq. (5.8). Hardening relation (2.7) is used with varying values of hardening index *n*. Predictions of Σ_P are practically identical.

pends on material hardening (softening) response and on elastic compressibility. The existence of a solution of Eq. (5.5) is of course a necessary condition for emergence of a plastic shock wave.

Specifying Eq. (5.5) for a given stress-strain curve, we find

$$8\beta\frac{d\eta}{d\Sigma} = (\eta+\beta)(3\eta-\beta)^2, \quad \eta = \frac{1}{h} = \frac{d\varepsilon}{d\Sigma} \tag{5.6}$$

The solution of Eq. (5.6) can be approximated by assuming that $\eta \gg \beta$

$$8\beta\frac{d\eta}{d\Sigma} \approx 9\eta^3 \tag{5.7}$$

and for the pure power hardening law Eq. (2.7), an approximate value of Σ_P is obtained from Eq. (5.7) in the form

$$\Sigma_P \approx \Sigma_y\left(\frac{8\beta(1-n)n}{9\Sigma_y}\right)^{n/(2-n)} \tag{5.8}$$

where $\Sigma_y = \sigma_y/E$ is the nondimensionalized yield stresses. Exact and approximate solutions, from Eqs. (5.6) and (5.8), are compared in Fig. 2. The deviation is hardly noticed, implying that relation (5.8) gives dependence of Σ_P on n quite accurately. For elastic/perfectly plastic materials, with $n=0$, Σ_P coincides with Σ_y.

The jump condition (3.3) implies that

$$\beta[\![\Sigma_r]\!] = -\frac{1}{2}(\beta[\![\Sigma]\!] + [\![\varepsilon]\!]) \approx -\frac{1}{2}(\beta+\eta_P)[\![\Sigma]\!] \tag{5.9}$$

with approximation $[\![\varepsilon]\!] \approx \eta_P[\![\Sigma]\!]$ where $\eta_P = d\varepsilon/d\Sigma$ is evaluated at Σ_P of Eq. (5.8). Assuming again that $\eta_P \gg \beta$ we find stress jump relation

$$[\![\Sigma_r]\!] \approx -\frac{\eta_P}{2\beta}[\![\Sigma]\!] \tag{5.10}$$

Further specification for the power law gives, by Eq. (5.8)

$$[\![\Sigma_r]\!] \approx -\frac{1}{2\beta n}\left(\frac{8\beta(1-n)n}{9\Sigma_y}\right)^{(1-n)/(2-n)}[\![\Sigma]\!] \tag{5.11}$$

This result shows that the ratio between the jumps in Σ and in Σ_r, at the discontinuity, is approximately independent of the cavity expansion velocity and can serve as a simple check of numerical results at the shock discontinuity. For common solids, the jump in radial stress predicted by Eq. (5.11) is much higher than the jump in Mises stress. A similar observation holds for the ratio $[\![\Sigma_h]\!]/[\![\Sigma]\!]$.

Table 1 Properties of investigated materials; m_C is the critical velocity at which the shock first appears

Material	ν	Σ_y	n	m_C
1	0.3	0.003	0.3	0.59
2	0.3	0.003	0.1	0.54
3	0.3	0.003	0.15	0.55
4	0.3	0.01	0.3	0.64
5	0.3	0.001	0.3	0.56
6	0	0.003	0.3	0.41
7	0.499	0.003	0.3	0.66

Returning to Eq. (5.1), specified on both sides of the shock

$$\beta m^2\xi_P^2 = \left.\frac{1+\beta h}{3-\beta h}e^{3\varepsilon+3\beta\Sigma_r+\beta\Sigma}\right|_{\xi=\xi_P^-,\xi_P^+} \tag{5.12}$$

and assuming that for common materials, $\varepsilon \gg \beta|\Sigma_r|$ in the vicinity of shock wave, we obtain a rough estimation of shock wave location.

$$\beta m^2\xi_P^2 \approx \left.\frac{1+\beta h}{3-\beta h}e^{3\varepsilon+\beta\Sigma}\right|_{\Sigma=\Sigma_P} \tag{5.13}$$

Thus, with Σ_P approximated by Eq. (5.8) we can assess through Eq. (5.13) the value of ξ_P for given material parameters (Σ_y, n).

It follows that shock jump conditions together with singularity condition (3.4) and density ratio equation (2.1)–the latter two imposed on both sides of ξ_P–enable numerical integration up to cavity wall $(\Sigma \to \infty)$ with the single unknown parameter C.

6 Numerical Results

Equations (2.3) and (2.4) have been integrated numerically employing a standard fourth-order Runge–Kutta method. Emergence of plastic shock wave has been controlled by checking the singularity condition (2.10) with increasing expansion velocity m. Once a singularity has been detected, integration was performed up to a close vicinity of ξ_P and continued across the shock wave with $(\xi_P^+ - \xi_P^-) \ll \xi_P$. Results have been obtained for several material types with parameters summarized in Table 1, along with the critical velocity at which the shock first appears (m_C) for each material. Results for material 1 are displayed in Figs. 2–6 for various values of m. In all figures discontinuities for $m > m_C$ are apparent, indicating the expected existence of plastic shock waves.

Over most of the range of ξ the values of the effective stress, shown in Fig. 3, are moderate; however, very close to the cavity

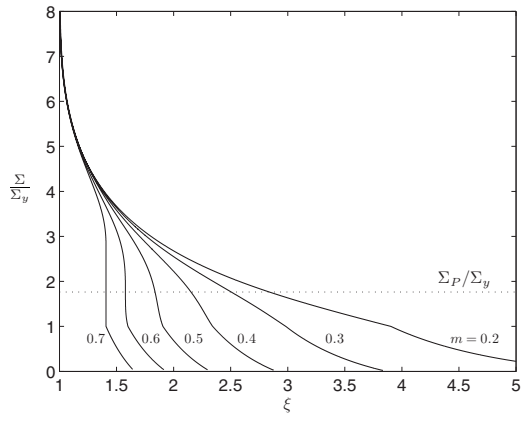

Fig. 3 Variation in effective stress along the radial coordinate ξ with different values of *m*, for material 1, as specified in Table 1. The dashed line shows the approximate value of Σ_P calculated from relation (5.8).

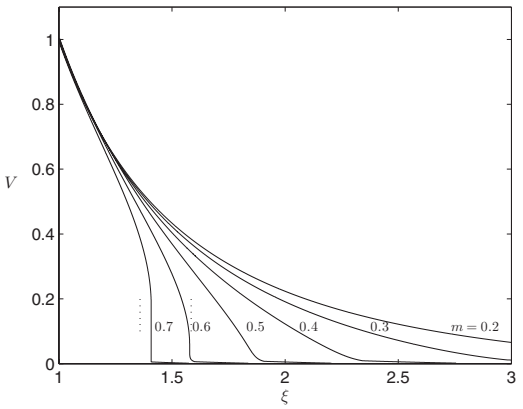

Fig. 4 Variation in V along the normalized radial coordinate ξ with different values of m for material 1, as specified in Table 1. The dashed lines represent the calculated values of ξ_P from relation (5.13), for $m=0.6, 0.7$, respectively.

wall there is a strong radial gradient, where $\Sigma/\Sigma_y \to \infty$, suggesting the existence of a near cavity boundary layer. The approximate value of Σ_P/Σ_y obtained from relation (5.8) is also represented in Fig. 3 revealing very good agreement for the intermediate value at the shock.

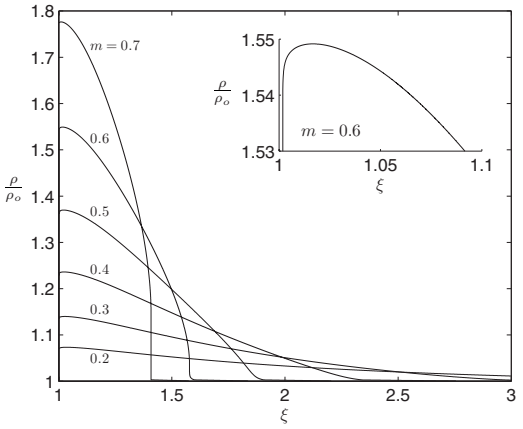

Fig. 5 Variation in density ratio ρ/ρ_o along the normalized radial coordinate ξ with different values of m for material 1, as specified in Table 1. Sub figure is enlargement of curve for $m=0.6$, showing the sharp drop in density near the cavity wall, indicating the existence of a boundary layer.

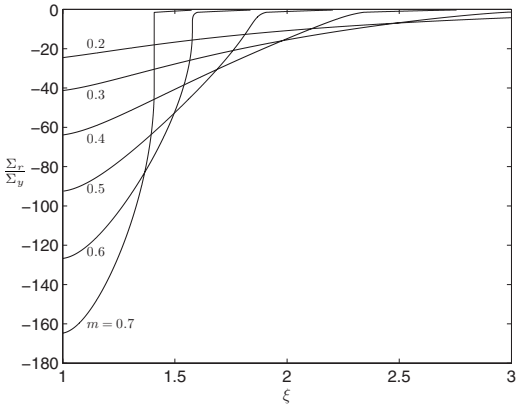

Fig. 6 Variation in radial stress along the normalized radial coordinate ξ with different values of m for material 1, as specified in Table 1

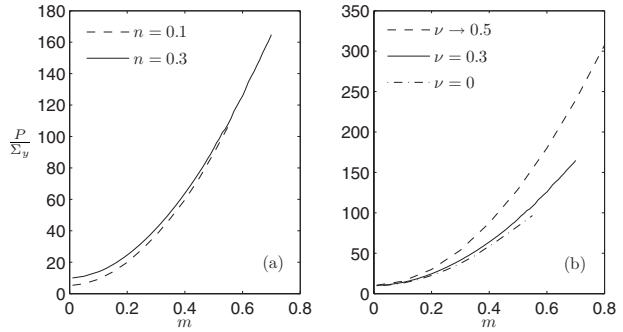

Fig. 7 Variation in applied pressure P with cavity expansion velocity for (*a*) materials 1 and 2 as specified in Table 1 (different values of hardening index n) and (*b*) materials 1, 6, and 7, as specified in Table 1 (different values of Poisson ratio ν)

In Fig. 4, the approximate values of ξ_P from relation (5.13) for $m=0.6$ and 0.7 are displayed along with radial profiles of the normalized velocity. For $m=0.6$, the approximate value of ξ_P is very accurate compared with the calculated value, however, as m increases the accuracy is reduced.

Clearly from Figs. 3 and 4, as the cavity expansion velocity increases, the extent of process zone (ξ_E), as well as the location of the plastic shock wave (ξ_P), decrease and severe gradients develop near the wall. This observation is in agreement with Eqs. (4.1) and (5.13), which indicate that both ξ_E and ξ_P behave like $1/m$. In fact, at high levels of m the ratio ξ_P/ξ_E depends, to leading terms, only on material properties. The order of locations $1 < \xi_P < \xi_i < \xi_E$ has been preserved in all cases examined in this study. However, with increasing levels of m the plastic shock moves toward the elastoplastic interface, eventually coinciding ($\xi_P = \xi_i$). In the absence of a smooth elastic-plastic transition, the shock will stay at ξ_i for higher cavity expansion velocities. However, for smooth hardening relations, such as the Ramberg–Osgood law, ξ_P continues to increase until, eventually, at very high levels of m, the elastoplastic shock coincides with the rigid/elastic interface ($\xi_P = \xi_E$).

Density profiles, in Fig. 5 show that over most of the range the density increases as the wall is approached. However, very close to the cavity wall, a maximum density is attained followed by a sudden drop, as shown by the enlarged curve, for $m=0.6$, in the sub figure. The strong changes in density, very close to the cavity wall, verify the existence of a near wall boundary layer.

Levels of shock intensity can be assessed from relative jumps in field variables across ξ_P. As expected, shock discontinuities become stronger with increasing expansion velocity (Figs. 3–6).

From the radial profile curves of Σ_r shown in Fig. 6, it is apparent that as m increases the radial stress approaches the cavity wall with steeper gradients and with extremely high levels of applied pressure, in a range where the ability of the material to endure these load levels becomes questionable. However, from Figs. 7 and 8, showing the dependence of the applied pressure on m for various material parameters, it is evident that the occurrence of a plastic shock wave does not radically change the behavior in terms of applied pressure. Curves of P versus m, similar to those of in Figs. 7 and 8, have been shown in Masri and Durban [1] but for a rather limited range of cavity expansion velocities that did not cover the formation of a plastic shock. Here, the sensitivity to ν is noticed (Fig. 7) at high expansion velocities while the hardening index and the yield stress have relatively little influence.

By comparison, we have plotted on Fig. 8 the dynamic branch of cavitation pressure formula for incompressible solids [1]

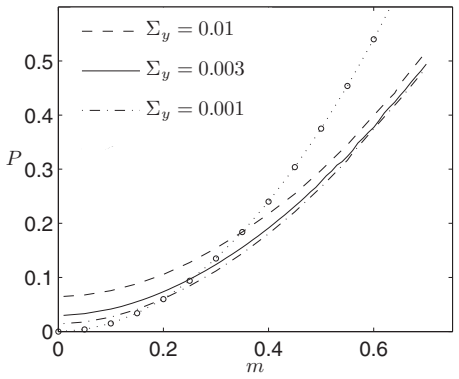

Fig. 8 Variation in applied pressure *P* with cavity expansion velocity for materials 1, 4, and 5, as specified in Table 1 (different values of Σ_y). Dynamic branch $3m^2/2$ for incompressible solids (ν=0.5) is shown by circles.

$$P = \int_0^\infty \frac{\Sigma d\varepsilon}{e^{3/2\varepsilon} - 1} + \frac{3}{2}m^2 \tag{6.1}$$

The deviation of $(P-P(m=0))$ from the classical Poncelet parabola $3m^2/2$ reflects influence of coupling between elastic compressibility and expansion velocity, implying that the Poncelet parabola is an upper bound on cavitation pressure, as illustrated in Fig. 8.

Curves for the constant C with varying values of m are shown in Fig. 9 for all materials from Table 1 with the known incompressible result $C=2/3$ recovered for any m.

The present self-similar solution applies to steady-state dynamic cavitation at high expansion velocities. It remains, although an open question whether the process of monotonously increasing the internal pressure inside the cavity will eventually induce a self-similar dynamic field under constant pressure.

The singular surface determined by Eq. (3.4) is associated with system equations (2.3) and (2.4) of ordinary nonlinear differential equations with no time coordinate as independent variable. The numerical results, supported by simple analysis of jump conditions across the plastic shock wave, reveal gradual development of an intense gradient zone as expansion velocity increases.

At critical values of m (about 3–4 km/s for common metals) a sharp discontinuity sets in and numerical procedure needs to account for Hugoniot conditions. Near wall boundary layer behavior obtained numerically compares well with asymptotic analysis given in next section.

For dynamic cavity expansion fields, that are not self-similar, we have the governing system of partial differential equations

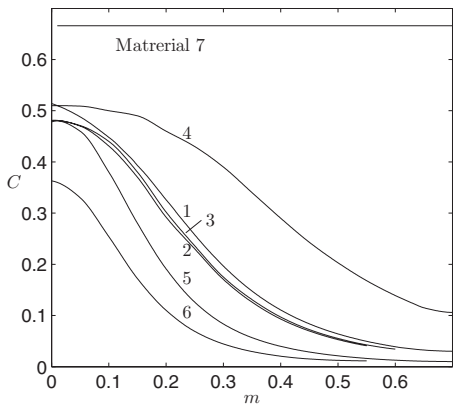

Fig. 9 Variation in *C* with cavity expansion velocity for materials specified in Table 1

$$\text{radial motion} \quad \frac{\partial \Sigma_r}{\partial R} + \frac{2}{R}(\Sigma_r - \Sigma_\theta) = \frac{\rho}{E}\frac{\partial U}{\partial t} \tag{6.2}$$

$$\text{radial strain rate} \quad \frac{\partial U}{\partial R} = \frac{\partial}{\partial t}(\Sigma_r - 2\nu\Sigma_\theta - \varepsilon_P) \tag{6.3}$$

$$\text{circumferential strain rate} \frac{U}{R} = \frac{\partial}{\partial t}\left(-\nu\Sigma_r + (1-\nu)\Sigma_\theta + \frac{1}{2}\varepsilon_P\right) \tag{6.4}$$

along with the density-pressure equation of state (2.1). Here, we denote by U the radial material velocity.

The characteristic slopes obtained from Eqs. (6.2)–(6.4) are

$$\beta\left(\frac{dR}{dt}\right)^2 = \left(\frac{E}{\rho}\right)\frac{1+\beta h}{3-\beta h} \tag{6.5}$$

in agreement with the small-strain ($\rho=\rho_o$) result [2]. A further substitution of Eqs. (2.1) and (2.5) results in

$$\beta m^2\left(\frac{dR}{\dot{A}dt}\right)^2 = \frac{1+\beta h}{3-\beta h}e^{\Theta} \tag{6.6}$$

which differs from the steady-state relation (2.10) by the term $\exp(2\Phi)$.

Now, subtracting Eq. (6.4) from Eq. (6.3) we get the equation

$$\frac{\partial U}{\partial R} - \frac{U}{R} = -\frac{\partial}{\partial t}\left((1+\nu)\Sigma - \frac{3}{2}\varepsilon_P\right) \tag{6.7}$$

Under steady-state conditions (Masri an Durban 2005) where $U = \dot{A}V$ and

$$\frac{\partial()}{\partial t} = \frac{\partial \xi}{\partial t}\frac{d()}{d\xi} = \frac{\dot{A}}{A}(V-\xi)\frac{d()}{d\xi} \tag{6.8}$$

Equation (6.7) integrates exactly to the holonomic form (2.2). Likewise, applying transformation (6.8) on R itself gives, with the aid of Eq. (2.2), in steady-state

$$\frac{dR}{dt} = -\dot{A}\xi e^{-\Phi} \tag{6.9}$$

Inserting Eq. (6.9) in Eq. (6.6), we find

$$\beta m^2 \xi^2 = \frac{1+\beta h}{3-\beta h}e^{\Theta+2\Phi} \tag{6.10}$$

which is identical with Eq. (2.10). Plastic shocks do not exist for incompressible solids, yet for $\beta \neq 0$ their existence should be confirmed by tracing the entire history of dynamic elastoplastic fields induced by an expanding cavity under monotonously increasing pressure.

7 Near Wall Boundary Layer Asymptotic Analysis

Near the cavity wall there exists a thin layer where the plastic branch dominates and, asymptotically $\varepsilon \gg \Sigma$ with $|\Sigma'|, |\Sigma_r'| \ll \varepsilon'$. Within this boundary layer, where $\xi \to 1$, the gradients in field variables (ρ, Σ) become significant, the density exhibits a sharp drop (Fig. 5), and the effective stress increases rapidly (Fig. 3), indicating the existence of an inner boundary layer. Under these assumptions within the boundary layer, the second of relation (2.2) can be approximated by

$$\Phi \sim \frac{3}{2}\varepsilon \tag{7.1}$$

so Eq. (2.3) is reduced to

$$\varepsilon' \sim \frac{2}{\xi}(1 - e^{\Phi}) \tag{7.2}$$

or after inserting relation (7.1) and integrating

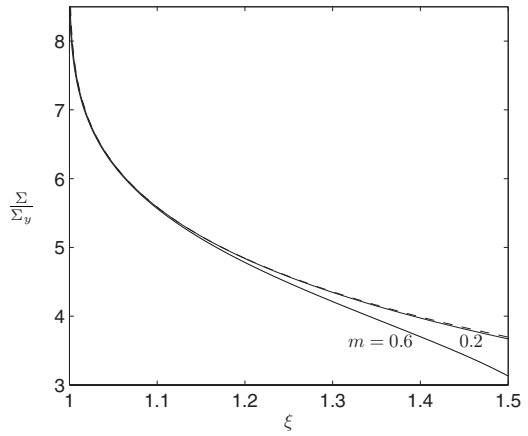

Fig. 10 Variation in Σ along the normalized radial coordinate ξ within the near cavity zone for material 1, as specified in Table 1, for $m=0.2,0.6$. The dashed line represents the asymptotic expansion (7.5).

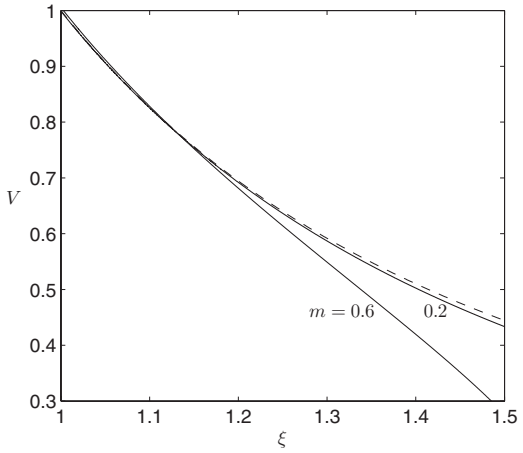

Fig. 11 Variation in V along the radial coordinate ξ within the near cavity zone for material 1, as specified in Table 1, for $m=0.2,0.6$. Dashed line represents the asymptotic expansion (7.6).

$$B\xi^3 \sim \frac{1}{1-e^{-(3/2)\varepsilon}} \tag{7.3}$$

where B is an integration constant. However, since $\varepsilon \to \infty$ as $\xi \to 1$ we have $B=1$ and Eq. (7.3) is simply

$$\varepsilon \sim \frac{2}{3}\ln\frac{\xi^3}{\xi^3-1} \tag{7.4}$$

independent of material parameters. Recalling that by Eq. (2.7) within the boundary layer $\Sigma \approx \Sigma_y^{1-n}\varepsilon^n$, we have the effective stress

$$\Sigma \sim \Sigma_y\left(\frac{2}{3\Sigma_y}\ln\frac{\xi^3}{\xi^3-1}\right)^n \tag{7.5}$$

This relation provides an asymptotic estimation for Σ within the boundary layer near the wall.

The boundary layer velocity profile V derived from relation (2.2), with the aid of Eq. (7.4), is simply the incompressible profile

$$V \sim \frac{1}{\xi^2} \tag{7.6}$$

Both asymptotic relations, for the effective stress and radial velocity, are independent of the cavity expansion velocity (m), although as shown in Figs. 10 and 11, accurate numerical results are better approximated for low cavity expansion velocities.

Turning to the asymptotic behavior of the radial stress, we start with the first-order approximation for Σ_r

$$\Sigma_r \sim -P + \Sigma_1(\xi-1), \quad \Sigma_1 = \Sigma_r'(\xi=1) \tag{7.7}$$

However, the radial equation of motion (2.4) can be written as

$$\Sigma_r' = \frac{2}{\xi}\Sigma + m^2\frac{\rho}{\rho_o}(V-\xi)V' \tag{7.8}$$

with the density ratio equation (2.1) rewritten, in terms of Σ_r and Σ, as

$$\frac{\rho}{\rho_o} = e^{-\beta(3\Sigma_r+2\Sigma)} \tag{7.9}$$

Now, at a distance from the wall we insert Eq. (7.7) in Eq. (7.9) to obtain the boundary layer approximation

$$\frac{\rho}{\rho_o} = e^{-2\beta\Sigma}e^{3\beta P}[1-3\beta\Sigma_1(\xi-1)] \tag{7.10}$$

Substituting Eqs. (7.6) and (7.10) in Eq. (7.8) results in, for $\xi \to 1$,

$$\Sigma_1(\xi-1) \sim \frac{\left(\Sigma + m^2e^{3\beta P-2\beta\Sigma}\dfrac{\xi^3-1}{\xi^4}\right)\dfrac{2(\xi-1)}{\xi}}{1+6\beta m^2e^{3\beta P-2\beta\Sigma}\dfrac{(\xi^3-1)(\xi-1)}{\xi^5}} \tag{7.11}$$

with Σ given by Eq. (7.5).

Boundary layer expansion for radial stress equation (7.7) and density equation (7.10) are now fully determined, for given m and P since Σ_1 is evaluated directly from Eq. (7.11). It can be seen from Figs. 12 and 13 that for a given value of P, the asymptotic behaviors of Σ_r and ρ/ρ_o are well captured, where again the approximation is better at low cavity expansion velocities.

8 Concluding Remarks

Spherical symmetric dynamic cavitation fields, at high expansion velocities, with propagation of plastic shock waves have been studied. Analysis is within framework of steady-state self-similar deformation patterns accounting for Hugoniot jump conditions across shock waves. Material behavior is according to J_2 plasticity theory with power hardening and elastic compressibility.

Solution within elastic field is approximated for small strains and an iterative numerical procedure is employed in post yield elastoplastic zone. Overall dependence of cavitation pressure on cavity expansion velocity shows little sensitivity to hardening in-

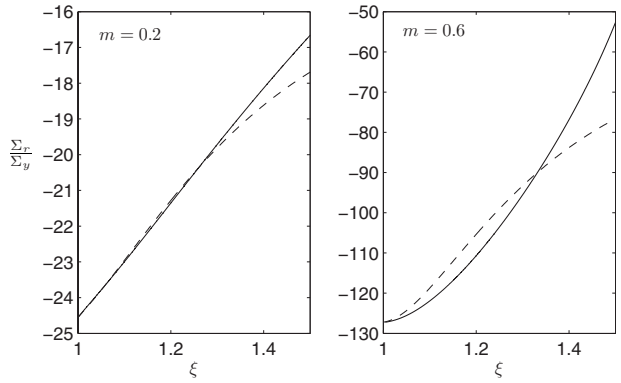

Fig. 12 Variation in Σ_r along the normalized radial coordinate ξ in the near cavity zone as specified in Table 1 with $m=0.2,0.6$. Dashed line represents the asymptotic approximation from relation (7.11).

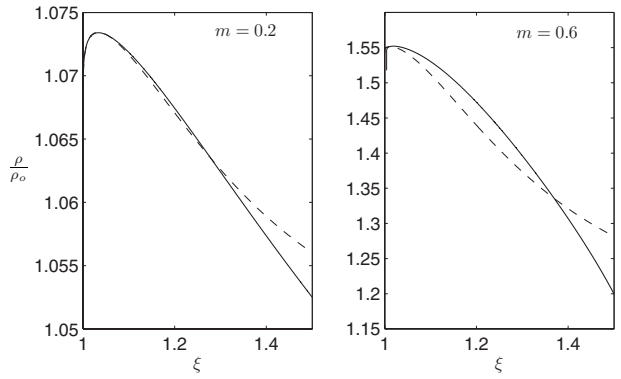

Fig. 13 Variation in ρ/ρ_o along the normalized radial coordinate ξ in the near cavity zone as specified in Table 1 with $m = 0.2, 0.6$. Dashed line represents the asymptotic approximation from relation (7.10).

dex. Very high levels of hydrostatic stress develop near the cavity wall with increasing expansion velocities while, by comparison, effective Mises stress attains much smaller values. An improved material model, which incorporates cut-off stress levels or a more realistic hydrostat (such as the Murnaghan power relation between Σ_h and ρ/ρ_o), or an internal damage law would probably clarify the near wall behavior at extremely high levels of pressure. Work in this direction is now pursued further (Cohen [7]) for porous materials.

Shock wave characteristics have been approximated by simple analytical expressions and, likewise, near wall boundary layer asymptotic analysis provides reasonable estimations in comparison with numerical results.

Acknowledgment

This research was supported by the Institute for Future Defense Technologies Research, named for Medvedi, Shwartzman, and Gensler Families.

References

[1] Masri, R., and Durban, D., 2005, "Dynamic Spherical Cavity Expansion in an Elastoplastic Compressible Mises Solid," ASME J. Appl. Mech., **72**, pp. 887–898.
[2] Hopkins, H. G., 1960, "Dynamic Expansion of Spherical Cavities in Metal," *Progress in Solid Mechanics*, I. N. Sneddon and R. Hill, eds., North-Holland, Amsterdam, Vol. 1.
[3] Hunter, S. C., and Crozier, R. J. M., 1968, "Similarity Solution for the Rapid Uniform Expansion of a Spherical Cavity in a Compressible Elastic-Plastic Solid," Q. J. Mech. Appl. Math., **21**, pp. 467–486.
[4] Luntz, Y. L., 1949, "The Propagation of Spherical Waves in an Elasto-Plastic Medium," Prikl. Mat. Mekh., **13**, pp. 55–78.
[5] Milne, P. C., and Morland, L. W., 1988, "A Continuous Loading Solution for Spherical Elastic-Plastic Waves of Small Amplitude," J. Mech. Phys. Solids, **36**(2), pp. 215–236.
[6] Durban, D., and Masri, R., 2004, "Dynamic Spherical Cavity Expansion in a Pressure Sensitive Elastoplastic Medium," Int. J. Solids Struct., **41**, pp. 5697–5716.
[7] Cohen, T., 2009, "Constitutive Aspects of Static and Dynamic Cavitation in Elastoplastic Solids," M.Sc. thesis, Technion.